



Biallelic mutations in *SORD* cause a common and potentially treatable hereditary neuropathy with implications for diabetes

Andrea Cortese^{1,2,3,37}✉, Yi Zhu^{4,5,37}, Adriana P. Rebelo^{1,37}, Sara Negri⁶, Steve Courel¹, Lisa Abreu¹, Chelsea J. Bacon⁷, Yunhong Bai⁷, Dana M. Bis-Brewer¹, Enrico Bugiardini², Elena Buglo¹, Matt C. Danzi¹, Shawna M. E. Feely⁷, Alkyoni Athanasiou-Fragkouli², Nourelhoda A. Haridy^{2,8}, Inherited Neuropathy Consortium*, Rosario Isasi¹, Alaa Khan^{2,9}, Matilde Laurà², Stefania Magri¹⁰, Menelaos Pipis², Chiara Pisciotta¹¹, Eric Powell¹, Alexander M. Rossor², Paola Saveri¹¹, Janet E. Sowden¹², Stefano Tozza¹³, Jana Vandrovцова², Julia Dallman¹⁴, Elena Grignani⁶, Enrico Marchioni¹⁵, Steven S. Scherer¹⁶, Beisha Tang¹⁷, Zhiqiang Lin¹⁸, Abdullah Al-Ajmi¹⁹, Rebecca Schüle^{20,21}, Matthias Synofzik^{20,21}, Thierry Maisonobe²², Tanya Stojkovic²³, Michaela Auer-Grumbach²⁴, Mohamed A. Abdelhamed⁸, Sherifa A. Hamed⁸, Ruxu Zhang¹⁸, Fiore Manganelli¹³, Lucio Santoro¹³, Franco Taroni¹⁰, Davide Pareyson¹¹, Henry Houlden², David N. Herrmann¹², Mary M. Reilly², Michael E. Shy⁷, R. Grace Zhai^{1,4,5}✉ and Stephan Zuchner¹✉

Here we report biallelic mutations in the sorbitol dehydrogenase gene (*SORD*) as the most frequent recessive form of hereditary neuropathy. We identified 45 individuals from 38 families across multiple ancestries carrying the nonsense c.757delG (p.Ala253GlnfsTer27) variant in *SORD*, in either a homozygous or compound heterozygous state. *SORD* is an enzyme that converts sorbitol into fructose in the two-step polyol pathway previously implicated in diabetic neuropathy. In patient-derived fibroblasts, we found a complete loss of *SORD* protein and increased intracellular sorbitol. Furthermore, the serum fasting sorbitol levels in patients were dramatically increased. In *Drosophila*, loss of *SORD* orthologs caused synaptic degeneration and progressive motor impairment. Reducing the polyol influx by treatment with aldose reductase inhibitors normalized intracellular sorbitol levels in patient-derived fibroblasts and in *Drosophila*, and also dramatically ameliorated motor and eye phenotypes. Together, these findings establish a novel and potentially treatable cause of neuropathy and may contribute to a better understanding of the pathophysiology of diabetes.

Hereditary neuropathies, also known as Charcot–Marie–Tooth disease (CMT), are clinically and genetically heterogeneous conditions affecting the peripheral nerves. CMT

is classified according to the motor conduction velocity in the upper-limb nerves as primarily demyelinating (CMT1) or axonal (CMT2). Distal hereditary motor neuropathy (dHMN) represents a

¹Dr. John T. Macdonald Foundation Department of Human Genetics and John P. Hussman Institute for Human Genomics, University of Miami Miller School of Medicine, Miami, FL, USA. ²Department of Neuromuscular Disease, UCL Queen Square Institute of Neurology and The National Hospital for Neurology, London, UK. ³Department of Brain and Behavioral Sciences, University of Pavia, Pavia, Italy. ⁴Department of Molecular and Cellular Pharmacology, University of Miami Miller School of Medicine, Miami, FL, USA. ⁵Program in Molecular and Cellular Pharmacology, University of Miami Miller School of Medicine, Miami, FL, USA. ⁶Istituti Clinici Scientifici Maugeri IRCCS, Environmental Research Center, Pavia, Italy. ⁷Department of Neurology, University of Iowa Carver College of Medicine, Iowa City, IA, USA. ⁸Department of Neurology and Psychiatry, Faculty of Medicine, Assiut University Hospital, Assiut, Egypt. ⁹Molecular Diagnostic Unit, Clinical Laboratory Department, King Abdullah Medical City in Makkah, Mecca, Saudi Arabia. ¹⁰Unit of Medical Genetics and Neurogenetics, Fondazione IRCCS Istituto Neurologico Carlo Besta, Milan, Italy. ¹¹Unit of Rare Neurodegenerative and Neurometabolic Diseases, Department of Clinical Neurosciences, Fondazione IRCCS Istituto Neurologico Carlo Besta, Milan, Italy. ¹²Department of Neurology, University of Rochester, Rochester, NY, USA. ¹³Department of Neuroscience, Reproductive Sciences and Odontostomatology, University of Naples “Federico II”, Naples, Italy. ¹⁴Department of Biology, University of Miami, Coral Gables, FL, USA. ¹⁵IRCCS Mondino Foundation, Pavia, Italy. ¹⁶Department of Neurology, Perelman School of Medicine, University of Pennsylvania, Philadelphia, PA, USA. ¹⁷Department of Neurology, Xiangya Hospital, Central South University, Changsha, China. ¹⁸Department of Neurology, The Third Xiangya Hospital, Central South University, Changsha, China. ¹⁹Division of Neurology, Department of Medicine, Al-Jahra Hospital, Al-Jahra, Kuwait. ²⁰Department of Neurodegenerative Disease, Hertie-Institute for Clinical Brain Research, and Center for Neurology, University of Tübingen, Tübingen, Germany. ²¹German Center of Neurodegenerative Diseases (DZNE), Tübingen, Germany. ²²Department of Neurophysiology, AP-HP, Sorbonne Université, Hôpital Pitié-Salpêtrière, Paris, France. ²³Centre de Référence des Maladies Neuromusculaires Nord/Est/Ile de France, AP-HP, Sorbonne Université, Hôpital Pitié-Salpêtrière, Paris, France. ²⁴Department of Orthopaedics and Traumatology, Medical University of Vienna, Vienna, Austria. ³⁷These authors contributed equally: Andrea Cortese, Yi Zhu, Adriana P. Rebelo. *A list of authors and their affiliations appears at the end of the paper. ✉e-mail: andrea.cortese@ucl.ac.uk; gzhai@med.miami.edu; szuchner@med.miami.edu

form of CMT2 in which the burden of disease falls predominantly or exclusively on motor nerves¹. In contrast to patients with CMT1, among whom more than 90% of individuals have mutations in known genes, only 20 to 30% of patients with CMT2 and dHMN receive a genetic diagnosis^{2,3}. Since up to 70% of CMT2 and dHMN cases are sporadic, identifying candidate pathogenic genes from single cases remains challenging even for next-generation sequencing techniques.

Results

Identification of biallelic *SORD* variants in undiagnosed inherited neuropathies. We took advantage of a large collection of over 1,100 patients with CMT for whom whole-exome sequencing (WES) and/or whole-genome sequencing (WGS) had been performed using the GENESIS analysis platform (<https://www.genesis-app.com>)⁴. We specifically looked for genes for which potentially pathogenic DNA variants were present in multiple families as well as for individual alleles over-represented in patients with CMT. By querying a subset of 598 patients undiagnosed with CMT for recessive nonsense variants in genes shared by >3 families and with a minor allele frequency (MAF) in the gnomAD control database of <1%, we identified 12 individuals from 11 unrelated families carrying a homozygous c.757delG (p.Ala253GlnfsTer27) variant in *SORD* (NM_003104.6) (GRCh38 15-45069018-CG-C; rs55901542). Four more individuals from three unrelated families carried the heterozygous p.Ala253GlnfsTer27 variant together with a second variant: c.298C>T (p.Arg100Ter) in family 2, c.329G>C (p.Arg110Pro) in family 3 and c.458C>A (p.Ala153Asp) in individuals II-1 and II-2 of family 14 (Fig. 1a–d, Extended Data Fig. 1 and Supplementary Table 2). All variants except that encoding p.Arg110Pro represented loss-of-function (LOF) alleles. Interestingly, the p.Arg110Pro change is adjacent to the previously reported p.Tyr111Phe (corresponding to p.Tyr110Phe in rats), which was shown to abolish *SORD* enzymatic activity and destabilize the protein⁵. Biallelic nonsense variants in *SORD* were absent from our internal disease controls (WES from 4,590 individuals affected by diverse neurological conditions but not CMT on the GENESIS platform).

SORD has a non-functional highly homologous paralog, the pseudogene *SORD2P*, which is thought to have arisen from the duplication of *SORD* within a 0.5-megabase region on chromosome 15 (Fig. 1e)⁶. Notably, the c.757delG (p.Ala253GlnfsTer27) variant in exon 7 of *SORD* is present in the pseudogene *SORD2P* in over 95% of control chromosomes, along with numerous additional exonic indel variants, which prevent effective translation of *SORD2P*^{7,8}. To specifically amplify *SORD*, but not *SORD2P*, in Sanger confirmation studies, we designed primers that took advantage of nucleotide sequence differences and distinct retrotransposon insertions in both genic regions (Supplementary Table 1). As a result of the high similarity of the regions, a nested PCR approach was necessary to

obtain specific amplification of exon 7 of *SORD* and distinguish it from the homologous region in *SORD2P*. We were able to confirm by Sanger sequencing the presence of the variants detected by WES or WGS in all individuals and provide segregation data in immediate-relative carriers (Fig. 1f and Extended Data Fig. 1).

We then screened an independent set of 103 unresolved CMT2/dHMN cases, for which WES had been performed at the UCL Institute of Neurology in London, UK, and identified 9 individuals from 6 unrelated families carrying the homozygous variant encoding p.Ala253GlnfsTer27 in *SORD* (8.7%). A third independent set of 297 patients with recessive or sporadic CMT2/dHMN was screened by Sanger sequencing of exon 7 of *SORD*; this was extended to the other coding exons when the p.Ala253GlnfsTer27-encoding allele was identified. This screening revealed 20 additional individuals (7%) from 18 families with biallelic variants in *SORD*: 16 individuals with a homozygous variant encoding p.Ala253GlnfsTer27 and 4 individuals with a variant encoding p.Ala253GlnfsTer27 in a compound heterozygous state with a second likely pathogenic variant. The last of these included a c.964G>A (p.Val322Ile) allele in family 29, a 275-base-pair deletion c.316_425+165del (p.Cys106Ter) in exon 4 in family 30, a de novo c.28C>T (p.Leu10Phe) change in family 32 and a c.895C>T (p.Arg299Ter) variant in family 33; all had a MAF of <0.0001 in gnomAD⁸. The residues affected by missense variants are highly conserved across multiple species (Fig. 1d) with GERP (genomic evolutionary rate profiling) scores greater than 3 (Supplementary Table 2).

The allelic carrier frequency of the variant encoding p.Ala253GlnfsTer27 in the control population is 0.004 based on an allelic count of 623 out of 142,588 genomes in the gnomAD v3 database⁸, ranging from 0.002 in the African and Asian populations to 0.005 in the European population, 0.007 in the Latin American population and up to 0.03 in the Amish population. Furthermore, there is only one male individual of East Asian ancestry in the gnomAD v3 database who is homozygous for the variant encoding p.Ala253GlnfsTer27 in *SORD*. Of note, in the previous gnomAD exome set (gnomAD v2.1.1), the p.Ala253GlnfsTer27 change was detected at a markedly lower rate (MAF=0.00008) due to failure to pass random forest filters. GENESIS uses the FreeBayes software for exome variant calling⁴, which may have resulted in an allele frequency (MAF_{GENESIS}=0.003; 27 alleles in 8,896 chromosomes) closer to that of the gnomAD v3 genome-based call set.

We further performed Sanger sequencing of 600 healthy controls, including 300 samples of European, 100 samples of Turkish and 200 samples of Middle Eastern origin, and identified 3 heterozygous, but no homozygous, p.Ala253GlnfsTer27-encoding alleles (MAF=0.0025). We identified p.Ala253GlnfsTer27 in patients of European, Asian and African ancestry with neuropathy, further rejecting the hypothesis of a historically recent founder mutation. In summary, these calculations

Fig. 1 | Biallelic mutations in *SORD* cause autosomal recessive dHMN/CMT2. **a**, Representative pedigrees of families with dHMN/CMT2 carrying biallelic mutations in *SORD*. A full set of pedigrees is provided in Extended Data Fig. 1. The squares indicate males and the circles indicate females. The diagonal line indicates an individual who had died. Patients are indicated with filled shapes. The plus symbols indicate the presence and the minus symbols indicate the absence of the mutant allele. **b**, A schematic diagram showing all exons, introns and UTRs of *SORD* based on the NCBI reference sequence NM_003104.6. The gray and white boxes represent the coding sequence and UTRs of *SORD*, respectively. The variants identified in the families with CMT considered in the present study map throughout the coding region of the gene. The nonsense variant c.757delG (p.Ala253GlnfsTer27) in exon 7, highlighted, was identified at a particularly high frequency. **c**, Distribution of variants across *SORD* protein domains. **d**, *SORD* protein ortholog alignments showing that the four missense substitutions identified in the families with dHMN/CMT2 in this study are located at highly conserved residues across species from humans to *Drosophila* (*Sodh2*). **e**, A schematic representation of *SORD* and its paralog *SORD2P*, thought to have arisen from the duplication of *SORD* within a 0.5-megabase region on chromosome 15. Highly homologous exonic regions between *SORD* and *SORD2P* are connected by dotted lines. **f**, Magnification of the nucleotide sequence of a highly homologous region in exon 7 in *SORD* (reverse strand) and *SORD2P* (forward strand). The G/C homopolymeric stretch, where the common c.757delG (p.Ala253GlnfsTer27) *SORD* variant is located, and the nucleotides in the flanking regions differing between *SORD2P* and *SORD*, are highlighted in red. Representative electropherograms show that the c.757delG (p.Ala253GlnfsTer27) *SORD* variant is found in a homozygous state in patients with dHMN/CMT2 (red box, lower plot) and in a heterozygous state in available parents (red box, upper plot), and is absent in the biallelic state from healthy controls (gray box) but is fixed in *SORD2P* (blue box).

support an estimated *SORD* neuropathy prevalence of ~1 per 100,000 individuals caused by a homozygous variant encoding p.Ala253GlnfsTer27 allele alone, making this specific variant the

most common individual pathogenic allele in the biallelic state in inherited neuropathies (Supplementary Table 3) and one of the most common alleles for any recessive Mendelian disease^{9,10}.

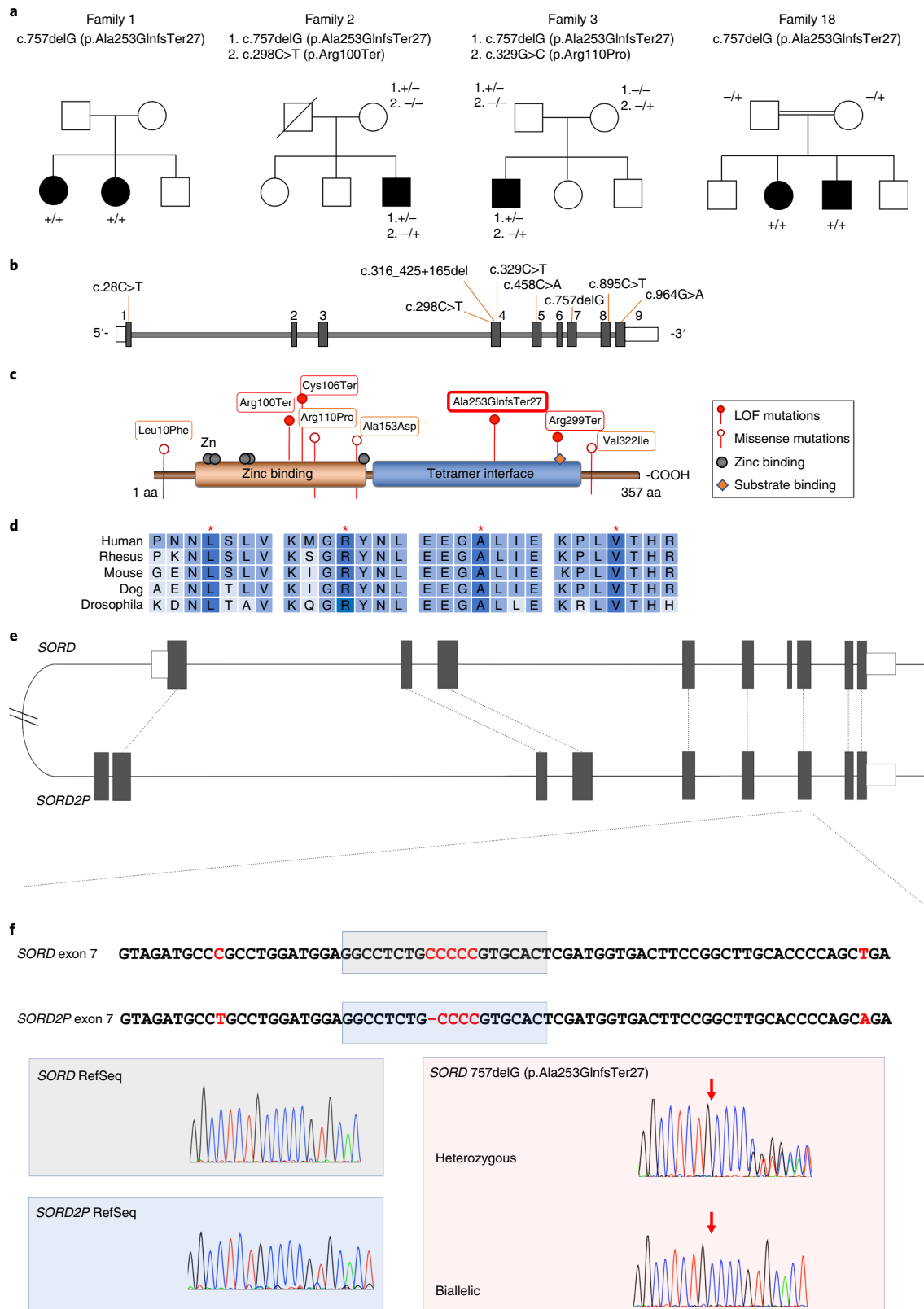


Table 1 | Clinical features of patients affected by hereditary neuropathy and carrying the biallelic mutations in *SORD*

Total individuals (n)	45
Number of males	32 (71%)
Age of onset (years)	Mean 17.2; s.d. 7.6; range 2–40
Age at examination (years)	Mean 34.3; s.d.13.1; range 15–70
Family history of neuropathy	14 (31%)
CMT subtype	
CMT2	23 (51%)
dHMN	18 (40%)
CMT intermediate	4 (9%)
Foot deformities	31 (69%)
Upper-limb weakness	
Proximal muscle groups	0/44 (0%)
Distal muscle groups	26/44 (59%)
Lower limb weakness	
Proximal muscle groups	2/44 (5%)
Distal muscle groups	43/44 (98%)
Prominent involvement of foot plantar flexion ^a	15/37 (41%)
Reduced vibratory sensation	17/40 (43%)
Reduced pinprick superficial sensation	13/39 (33%)
Disease severity	
Mild	30 (67%)
Moderate	14 (31%)
Severe	1 (2%)
Use of ankle-foot orthoses	19 (42%)
Other walking aids	2 (4%)
Nerve conduction study	
Reduced motor conduction velocity	11/42 (26%)
Reduced sensory action potentials	26/40 (65%)

Categorical data are expressed as n (%) if data are available in all individuals or n/number of individuals considered (%). Continuous variables are expressed as mean; s.d.; range. ^aFoot plantar flexion equal to or weaker than foot dorsal flexion.

Clinical features of patients with *SORD* neuropathy. Altogether, we identified 45 individuals from 38 unrelated families with biallelic mutations in *SORD* (Table 1 and Supplementary Table 4). Of note, 69% of cases were sporadic, with no evidence of a family history or consanguinity, but the patients were clinically diagnosed as having CMT on the basis of the presence of a slowly progressive neuropathy, often accompanied by foot deformities. The formal clinical diagnosis was axonal CMT in 51% ($n=23$), dHMN in 40% ($n=18$) and intermediate CMT in 9% ($n=4$) of individuals. The mean age of onset of the neuropathy was 17 ± 8 years and difficulty walking was the most common complaint at onset. Delayed motor milestones were uncommon, but two-thirds of the patients reported foot deformities, indicating that the neuropathy probably started earlier in life. All individuals had limb weakness, but only one-half had sensory impairment. Weakness was mild in distal upper limbs and ranged from mild to near-complete paralysis in the distal lower limbs. The proximal muscles of the upper and lower limbs were typically unaffected. Seven patients had upper-limb tremor, four had mild scoliosis and two had mild hearing loss. One patient (individual 14) had a concurrent and likely unrelated

syndromic disorder encompassing dysmorphic features and static encephalopathy from the age of 3 years, and spastic ataxia with evidence of cerebellar atrophy on magnetic resonance imaging of the brain. Another patient (individual 36), carrying a compound heterozygous p.Ala253GlnfsTer27/p.Val322Ile genotype, presented with earlier onset of the disease and severe neuropathy. The variant encoding p.Val322Ile was not identified in any other patient of this study, is present in three individuals in gnomAD and has conflicting in silico predictions from tolerated to disease-causing. None of the patients had cataracts or involvement of other organs. With the CMT neuropathy score (CMTNSv2)¹¹, after 17 ± 11 years of disease duration the neuropathy was mild in 67% ($n=30$), moderate in 31% ($n=14$) and severe in 1 patient. Ankle-foot orthosis during walking was used by 42% of patients ($n=19$); 1 patient required unilateral support and 1 patient was wheelchair-dependent. Detailed nerve conduction studies were available in 42 patients and invariably showed a motor axonal neuropathy, with intermediate reduction of conduction velocities in 26% of patients ($n=11$, mean conduction velocity in upper limbs = $39 \pm 3 \text{ m s}^{-1}$, range $32\text{--}42 \text{ m s}^{-1}$) and decreased or absent amplitudes of sensory action potentials in 26% of patients ($n=11$).

Loss of *SORD* enzymatic activity and increased serum fasting sorbitol level. *SORD* is a homotetramer of 38-kDa subunits and is widely expressed in mammalian tissues^{5,12,13}. It is the second enzyme of the two-step polyol pathway, in which aldose reductase converts glucose into sorbitol, a relatively non-metabolizable sugar, which is then oxidized to fructose by *SORD* (Fig. 2a). To gather further insights into the functional consequences of biallelic mutations in *SORD*, we next assessed *SORD* protein expression in fibroblasts from four independent healthy controls compared to four unrelated affected individuals homozygous for the variant encoding p.Ala253GlnfsTer27, one patient with compound p.Ala253GlnfsTer27/p.Arg299Ter-encoding variants and two unaffected heterozygous carriers of the variant encoding p.Ala253GlnfsTer27. The *SORD* protein was absent in all patients, and the *SORD* levels were reduced in unaffected carriers compared to controls (Fig. 2b). Accordingly, intracellular sorbitol concentrations were over 10 times higher in patient-derived fibroblasts compared to controls (Fig. 2c). We next tested the fasting sorbitol level in serum from 10 patients carrying the homozygous variant encoding p.Ala253GlnfsTer27 and 10 unrelated controls and found that it was over 100 times higher (14.82 ± 0.780 versus $0.046 \pm 0.004 \text{ mg l}^{-1}$, $P < 0.0001$), confirming the lack of *SORD* enzymatic activity in patients (Fig. 2d).

***Drosophila melanogaster* model of *SORD* deficiency recapitulates the disease phenotype.** To further explore the pathophysiology of *SORD* mutations in vivo, we established *Drosophila melanogaster* models of *SORD* deficiency (Fig. 3). *Drosophila* has two functional *Sord* proteins—*Sodh1* (NP_001287203.1) and *Sodh2* (NP_524311.1)—that are 75% and 73% identical to the human *SORD* protein (NP_003095.2), respectively, and 90% identical to each other¹⁴. We obtained the *Sodh2*^{MB01265} mutant allele of *Sodh2* in which a transposon disrupts the gene¹⁵. Homozygous *Sodh2* (*Sodh2*^{MB01265/MB01265}) mutants are viable with a normal lifespan (Extended Data Fig. 2), and as described later, 10 days after eclosion (DAE) the sorbitol level was significantly increased in the fly heads (Fig. 4b), consistent with our observations in patient-derived fibroblasts. To determine whether *Sodh2*^{MB01265/MB01265} mutants had a neurodegenerative phenotype, we examined the visual system, in which subtle neuronal and synaptic pathological changes can be detected¹⁶. Axons of the outer photoreceptors traverse the lamina cortex and make synaptic connections with lamina monopolar neurons (Fig. 3a). In the control (yw) flies at 2 DAE, the lamina cartridges of photoreceptor synapses can be visualized in the x - y and x - z planes (Fig. 3b). We observed a loss of photoreceptor

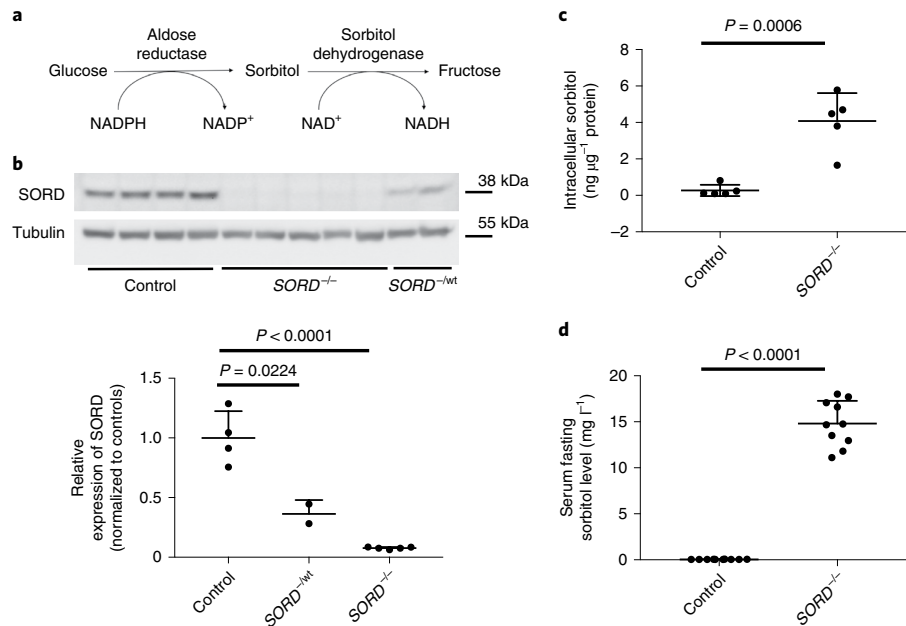


Fig. 2 | Decreased SORD expression and sorbitol accumulation in patients. **a**, A schematic representation of the two-step polyol pathway converting glucose to fructose. **b**, A representative cropped immunoblot (top) and corresponding graph (bottom) showing the levels of SORD and tubulin protein in healthy controls ($n=4$, lanes 1–4), patients carrying nonsense mutations in *SORD* ($n=5$, homozygous for the variant encoding p.Ala253GlnfsTer27 in lanes 5–8 and compound heterozygous p.Ala253GlnfsTer27/p.Arg299Ter-encoding variants in lane 9) and heterozygous carriers of p.Ala253GlnfsTer27 ($n=2$, lanes 10 and 11). Uncropped gels are provided as source data. **c**, Levels of intracellular sorbitol were measured by ultraperformance liquid chromatography (UPLC) and normalized to protein content in cultured fibroblasts from unrelated healthy controls ($n=5$) and patients carrying biallelic p.Ala253GlnfsTer27-encoding mutations in *SORD* ($n=5$). **d**, The fasting sorbitol level in serum from unrelated healthy controls ($n=10$) and patients carrying biallelic p.Ala253GlnfsTer27-encoding mutations in *SORD* ($n=10$). The graphs show the mean \pm standard deviation (s.d.; error bars) and data distribution (dots), and the P value of two-tailed t -tests comparing SORD protein and sorbitol levels across groups. All experiments were repeated independently twice with similar results.

terminals in the lamina layer of *Sodh2*^{MB01265/MB01265} mutants at 2 DAE (Fig. 3c)—visualized as vacuole-like structures of reduced fluorescence after labeling with antibodies against neuronal membranes (horseradish peroxidase (HRP)) and synaptic active zones (bruchpilot (BRP); Fig. 3c,d). This phenotype was more severe at 10 DAE, with more numerous and larger vacuole-like structures distributed across the synaptic lamina layer (Fig. 3c,d). To validate our findings, we generated a second model by neuronal-specific knockdown of both *Sodh1* and *Sodh2*, resulting in age-dependent formation of vacuole-like structures (Extended Data Fig. 3) similar to that of the *Sodh2*^{MB01265/MB01265} flies. We also found that the locomotor activities of both LOF models were significantly worse than that of the control (*yw*) flies at a late stage (40 DAE) (Fig. 3e,f), consistent with the progressive, age-dependent neuromuscular dysfunction seen in our patients. Taken together, *Drosophila* models of SORD deficiency recapitulate key phenotypes in the patients, including a normal lifespan and progressive and age-dependent synaptic degeneration and locomotor deficiency.

Treatment with aldose reductase inhibitors normalizes intracellular sorbitol and rescues the phenotype in *Drosophila melanogaster*. We investigated the possibility that *SORD*-associated hereditary neuropathy could be treated. Pharmacological inhibition of aldose reductase, the enzyme upstream of SORD, has been shown to reduce detrimental sorbitol accumulation in cellular and animal model of diabetes^{17–21} and in humans^{22–24}. We thus tested the effect of two commercially available aldose reductase inhibitors, epalrestat and ranirestat, on intracellular sorbitol accumulation in patient-derived fibroblasts lacking functional SORD. Patient-derived and control

fibroblasts were grown for 72 h in the presence or absence of epalrestat (100 μ M) or ranirestat (10 μ M) and intracellular sorbitol levels were measured thereafter. In patient-derived fibroblasts, both epalrestat and ranirestat significantly reduced sorbitol levels (Fig. 4a).

Next, we fed the *Drosophila* models of SORD deficiency with epalrestat (80 μ g ml⁻¹) and ranirestat (80 μ g ml⁻¹) or the vehicle dimethylsulfoxide (DMSO) starting at 2 DAE. At 10 DAE, the heads of DMSO-treated *Sodh2*^{MB01265/MB01265} flies had significantly increased sorbitol levels, but treatment with either epalrestat or ranirestat was able to reduce the sorbitol levels to those observed in control (*yw*) flies (Fig. 4b). Epalrestat or ranirestat rescued the locomotor activities of both *Sodh2*^{MB01265/MB01265} flies and flies with neuronal-specific knockdown of both *Sodh1* and *Sodh2* to the levels of control (*yw*) flies (Fig. 4c and Extended Data Fig. 4) and restored the age-dependent synaptic defects in *Sodh2*^{MB01265/MB01265} mutant flies by reducing the number of vacuole-like structures and restoring the localization of the synaptic cytomatrix protein BRP at both 10 and 40 DAE (Fig. 4d–g). In contrast, the loss of synaptic termini was so advanced in DMSO/vehicle-treated flies at 40 DAE that neighboring vacuoles fused to form much larger vacuole-like structures that encompassed multiple synaptic cartridges (Fig. 4d).

Discussion

We show that biallelic *SORD* mutations are a novel cause of inherited neuropathy. Genetic data from our cohort as well as from control databases suggest that the predominant pathogenic variant in *SORD*, c.757delG (p.Ala253GlnfsTer27), with a carrier frequency of ~ 3 per 1,000 individuals, is the most common recessive cause of neuropathy identified to date and represents one of the most

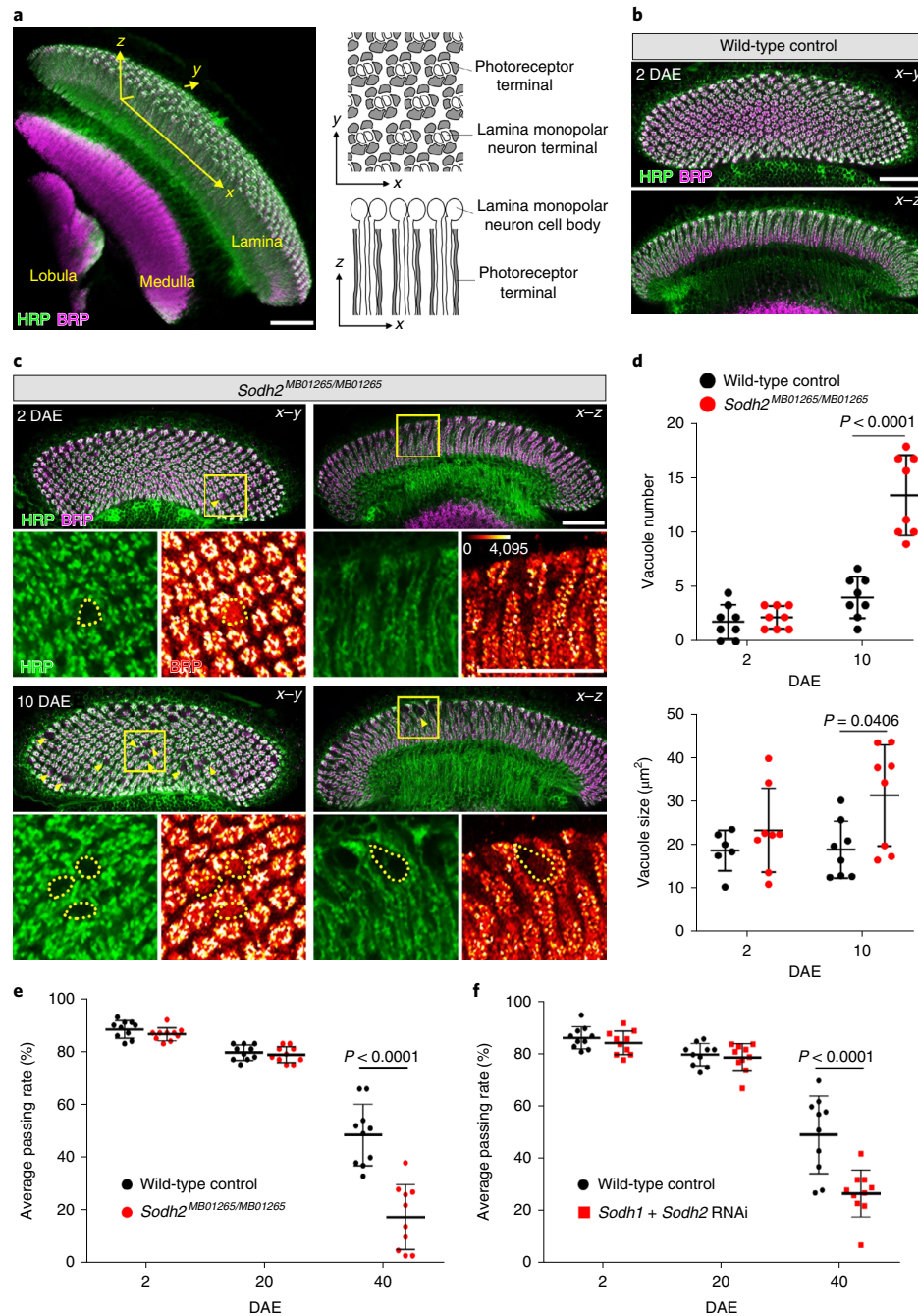


Fig. 3 | Loss of *Drosophila* *Sodh2* causes age-dependent synaptic degeneration. **a**, The three-dimensional structure of the *Drosophila* visual system stained with HRP (green; marks neuronal membranes) and (BRP, magenta; marks synaptic active zones), showing the lamina, medulla and lobula. The *x-y* and *x-z* planes showing the photoreceptor terminals and lamina neurons are indicated. Scale bar, 30 μm . **b**, Optical sections of the laminae of *yw* control flies at 2 DAE, stained with HRP (green) and BRP (magenta). The organized lamina cartridges and columnar photoreceptor neurons are shown in the *x-y* and *x-z* planes, respectively. Scale bar, 30 μm . **c**, Optical sections of the laminae at the level of the terminals of *Sodh2*^{MB01265/MB01265} homozygous flies at 2 DAE and 10 DAE, stained with HRP (green) and BRP (magenta). The yellow arrowheads indicate the lamina vacuole-like structures that correspond to missing terminals. The areas outlined by yellow boxes are shown at a higher magnification. The intensity of BRP is indicated using a red spectrum. The dotted lines indicate the area of lamina vacuole-like structures. Scale bars, 30 μm . **d**, Quantification of the number (top) and size (bottom) of the vacuole-like structures. $n = 8$ biologically independent samples. The data are presented as mean \pm s.d. (error bars). Statistical analysis was performed using two-way analysis of variance (ANOVA) followed by post hoc Tukey's multiple-comparison test. **e, f** Locomotor activity of control flies (*yw*) and *Sodh2*^{MB01265/MB01265} flies (**e**) or *Sodh1* and *Sodh2* pan-neuronal double knockdown (RNA interference (RNAi)) (**f**) flies. $n = 10$ biologically independent experiments. The data are presented as mean \pm s.d. (error bars). Statistical analysis was performed using two-way ANOVA followed by post hoc Tukey's multiple-comparison test.

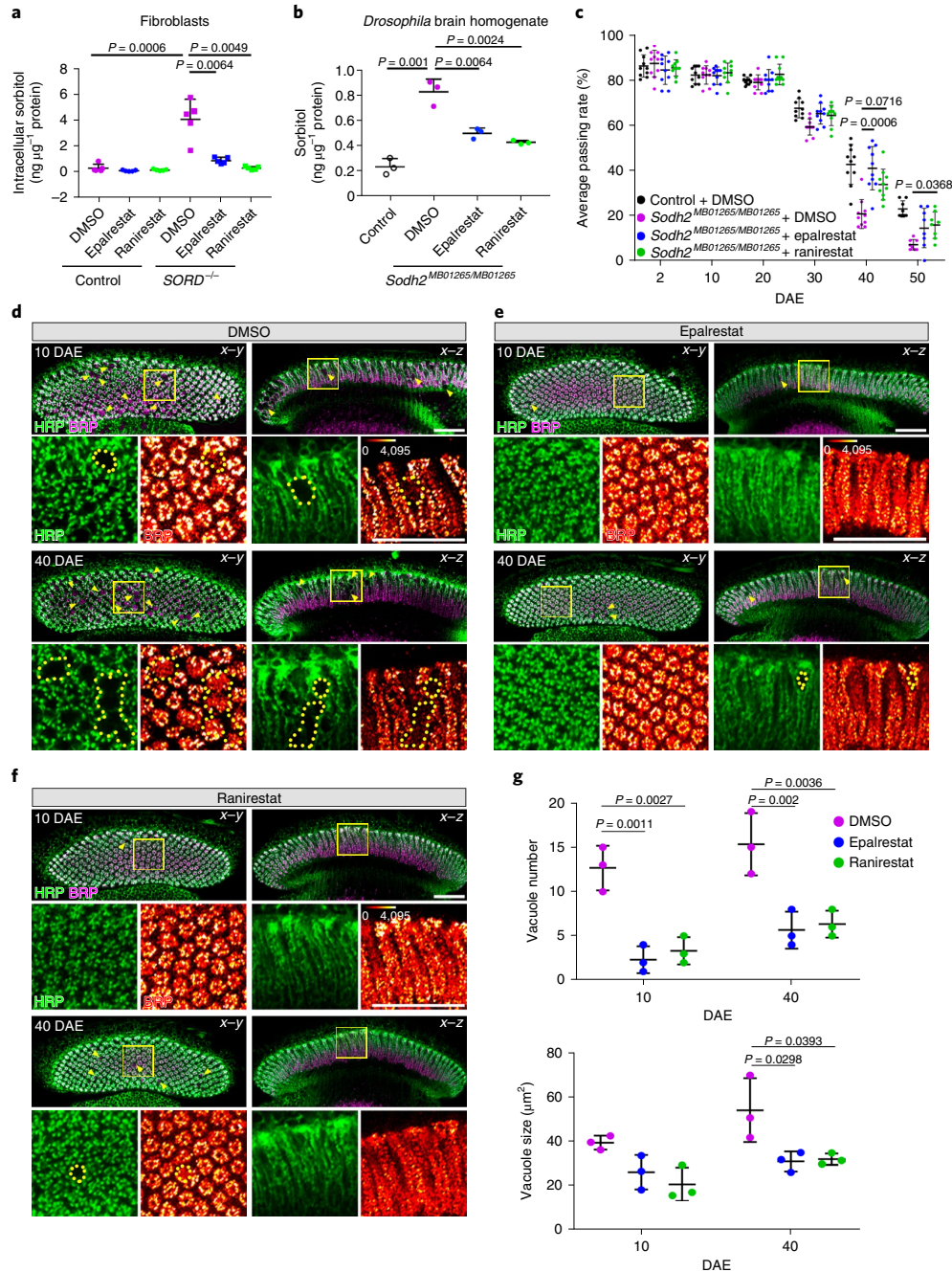


Fig. 4 | Treatment with aldose reductase inhibitors epalrestat and ranirestat decreases sorbitol levels and prevents functional losses. a, Intracellular sorbitol levels were measured by UPLC and normalized to protein content in fibroblasts from healthy controls ($n = 5$, circles) and patients carrying biallelic nonsense mutations in *SORD* ($n = 5$, squares) after 3 days of treatment with 100 μM epalrestat, 10 μM ranirestat or DMSO. **b**, Sorbitol levels were measured in brain/head homogenates and normalized to protein concentration from wild-type (*yw*) ($n = 3$) and *Sodh2*^{MB01265/MB01265} ($n = 3$) flies at 10 DAE. *Sodh2*^{MB01265/MB01265} flies were fed epalrestat ($n = 3$) or ranirestat ($n = 3$) at a final concentration of 80 $\mu\text{g ml}^{-1}$, or DMSO. The graphs show the mean \pm s.d. (error bars). A two-tailed t-test was performed to compare the sorbitol level. Sorbitol measurement was repeated twice with similar results. **c**, Locomotor activity of control flies (*yw*) fed with DMSO, *Sodh2*^{MB01265/MB01265} flies fed with DMSO, 80 $\mu\text{g ml}^{-1}$ epalrestat or 80 $\mu\text{g ml}^{-1}$ ranirestat. $n = 10$ biologically independent experiments at 2, 10, 20, 30 and 40 DAE, and $n = 8$ at 50 DAE. The data are presented as mean \pm s.d. (error bars). Statistical analysis was performed using two-way ANOVA followed by post hoc Tukey's multiple-comparison test. **d-f**, Laminae of *Sodh2*^{MB01265/MB01265} homozygous flies at 10 DAE and 40 DAE fed with DMSO (**d**), 80 $\mu\text{g ml}^{-1}$ epalrestat (**e**) or 80 $\mu\text{g ml}^{-1}$ ranirestat (**f**) were stained with HRP (green) and BRP (magenta). The yellow arrowheads indicate the lamina vacuole-like structures. The areas outlined by yellow boxes are shown at a higher magnification. The intensity of BRP is indicated using a red spectrum. The dotted lines indicate the area of lamina vacuole-like structures. Scale bars, 30 μm . **g**, Quantification of the number (top) and size (bottom) of the vacuole-like structures (**d-f**). $n = 3$ biologically independent animals. The data are presented as mean \pm s.d. (error bars). Statistical analysis was performed using two-way ANOVA followed by post hoc Tukey's multiple-comparison test.

common specific alleles causing a recessive Mendelian disease. Indeed, with a frequency in undiagnosed CMT2 and dHMN cases of up to ~10%, the variant encoding p.Ala253GlnfsTer27 will probably account for a substantial portion of the diagnostic gap in inherited axonal neuropathies, rivaled only by the common dominant CMT2 gene *MFN2* (ref. 25). It is intriguing that, despite their frequency, mutations in *SORD* were not previously identified as a cause of CMT. We speculate that widely used next-generation sequencing analysis pipelines had difficulties to call variants in *SORD* in the presence of the homologous *SORD2P* pseudogene. Other known pathogenic variants have previously been shown to be concealed by the presence of pseudogenes²⁶. It is tempting to speculate that the appearance of the common c.757delG (p.Ala253GlnfsTer27) pathogenic allele could have arisen from interlocus gene conversion between *SORD2P*, where c.757delG is fixed in the absence of selective pressure, and *SORD*. Indeed, interlocus gene conversion is increasingly recognized as a mechanism causing human inherited disease^{27–29}. If this hypothesis is confirmed, it would offer an intriguing mechanistic parallelism placing nonallelic homologous recombination, resulting in unequal crossover, as in *PMP22* duplication/deletion causing CMT1A³⁰, and gene conversion of *SORD* at the center of the most common forms of demyelinating and axonal CMT, respectively. However, no other nucleotide was changed in the nearby region of *SORD* to resemble the *SORD2P* sequence. Therefore, a single-base deletion resulting from DNA replication errors along this homopolymeric repeat of G/C nucleotides, independently occurring in both *SORD* and *SORD2P*, could also represent an alternative and valid hypothesis.

The pathogenicity of *SORD* mutations is further supported by the in vitro data for patient-derived fibroblasts, which showed absent *SORD* protein and intracellular sorbitol accumulation, and the dramatically higher fasting sorbitol level in the serum of patients, which itself represents a promising biomarker for this condition. Two in vivo *Drosophila* models recapitulated key aspects of the human phenotype—increased sorbitol levels, and progressive synaptic degeneration and motor impairment. We propose enzymatic LOF and subsequent sorbitol accumulation as the mechanism of action for *SORD*-associated CMT. This conclusion is in accord with the finding that pharmacological inhibitors of *SORD* worsen neuropathy in diabetic rats^{31,32}.

Our findings do not fully elucidate the mechanism of axonal damage caused by *SORD* deficiency: one or more of the known effects of decreased *SORD* activity, including increased levels of sorbitol and cellular osmolarity, oxidative stress and decreased NADPH levels, are plausible^{33,34}. Mice that have markedly reduced levels of *SORD* protein due to an intronic splicing mutation (C57BL/LiA mice), bred and fed according to the standard laboratory conditions, do not develop neuropathy or even slowed nerve conduction velocities^{35–37}. This is possibly due to a difference in sugar metabolism between humans and mice since standard mouse chow consists of a low-sugar diet compared to that of humans³⁸ and flies, which are fed on a sugar-based diet. Indeed, *SORD* deficiency does aggravate the cataract formation and neuropathy in rodent models of diabetes^{31,36,37}. On the basis of clinical data from patients and the late-onset phenotype observed in flies, it will be important to examine aging C57BL/LiA mice, or test the effect on the peripheral nerves of a higher sugar consumption, as well as create other models of *SORD* deficiency.

Our study further unravels a central role of the polyol pathway in peripheral nerve metabolism and survival in normoglycemic conditions. Although the mechanism by which increased intracellular sorbitol leads to selective degeneration of peripheral axons is yet unknown, the observation of increased sorbitol levels in patient-derived cells in this study has promising implications, both as a biomarker of *SORD*-associated CMT and as a target for future therapeutic interventions, including methods for substrate

reduction, gene replacement or correction, and *SORD* enzyme substitution. Accordingly, we have demonstrated in preclinical studies the beneficial effects of substrate reduction via the application of aldose reductase inhibitors in human-derived cells and *Drosophila* models. Epalrestat is currently marketed in a few countries for the treatment of diabetic complications²¹ while ranirestat has been advanced into late stages of clinical trials^{23,24}. Both drugs showed a good safety profile in patients with diabetic neuropathy. Whether those drugs may also represent a safe and effective approach for the treatment of *SORD*-associated inherited neuropathy, given their known risk of off-target effects and inducing more widespread metabolic alterations, will need to be addressed by future studies.

Finally, as an example of rare diseases informing common health issues, the identification of *SORD*-associated neuropathy may have broader implications to the field of diabetic neuropathy and retinopathy. Diabetes represents the most frequent cause of neuropathy in Western countries, affecting 30–60% of patients with diabetes and 20–30 million people worldwide^{39,40}. Its pathogenesis is exceptionally complex, and available treatments are mostly symptomatic. Increased polyol pathway flux has been reported to cause osmotic damage and oxidative stress to retinal cells, including neurons, Müller glia, pericytes and vascular endothelial cells. Aberrant retinal sorbitol accumulation can lead to microvascular damage and subsequent neovascularization⁴¹. However, the direct impact of sorbitol accumulation on photoreceptor neurons is not well characterized. Our fly models of *SORD* deficiency show the age-dependent formation of vacuole-like structures and reduced synaptic proteins, indicating that an increased sorbitol level in the retina can have a direct detrimental effect on the photoreceptor neurons and contribute to retinal phenotypes in diabetic retinopathy. Further elucidation of the process leading to nerve degeneration in the constituent absence of *SORD* will hopefully translate into a better understanding of the composite mechanisms underlying the onset and progression of diabetic neuropathy and retinopathy.

Online content

Any methods, additional references, Nature Research reporting summaries, source data, extended data, supplementary information, acknowledgements, peer review information; details of author contributions and competing interests; and statements of data and code availability are available at <https://doi.org/10.1038/s41588-020-0615-4>.

Received: 4 November 2019; Accepted: 20 March 2020;
Published online: 4 May 2020

References

- Rossor, A. M., Tomaselli, P. J. & Reilly, M. M. Recent advances in the genetic neuropathies. *Curr. Opin. Neurol.* **29**, 537–548 (2016).
- Fridman, V. et al. CMT subtypes and disease burden in patients enrolled in the Inherited Neuropathies Consortium natural history study: a cross-sectional analysis. *J. Neurol. Neurosurg. Psychiatry* **86**, 873–878 (2015).
- Cortese, A. et al. Targeted next-generation sequencing panels in the diagnosis of Charcot-Marie-Tooth disease. *Neurology* **94**, e51–e61 (2020).
- Gonzalez, M. et al. Innovative genomic collaboration using the GENESIS (GEM.app) platform. *Hum. Mutat.* **36**, 950–956 (2015).
- Hellgren, M., Kaiser, C., de Haij, S., Norberg, A. & Höög, J.-O. A hydrogen-bonding network in mammalian sorbitol dehydrogenase stabilizes the tetrameric state and is essential for the catalytic power. *Cell. Mol. Life Sci.* **64**, 3129–3138 (2007).
- Carr, A. S. et al. A study of the neuropathy associated with transthyretin amyloidosis (ATTR) in the UK. *J. Neurol. Neurosurg. Psychiatry* **87**, 620–627 (2016).
- 1000 Genomes Project Consortium et al. A global reference for human genetic variation. *Nature* **526**, 68–74 (2015).
- Lek, M. et al. Analysis of protein-coding genetic variation in 60,706 humans. *Nature* **536**, 285–291 (2016).
- Lazarin, G. A. et al. An empirical estimate of carrier frequencies for 400+ causal Mendelian variants: results from an ethnically diverse clinical sample of 23,453 individuals. *Genet. Med.* **15**, 178–186 (2013).

10. Antonarakis, S. E. Carrier screening for recessive disorders. *Nat. Rev. Genet.* **20**, 549–561 (2019).
11. Murphy, S. M. et al. Reliability of the CMT neuropathy score (second version) in Charcot-Marie-Tooth disease. *J. Peripher. Nerv. Syst.* **16**, 191–198 (2011).
12. Johansson, K. et al. Crystal structure of sorbitol dehydrogenase. *Chem. Biol. Interact.* **130–132**, 351–358 (2001).
13. Lindstad, R. I., Teigen, K. & Skjeldal, L. Inhibition of sorbitol dehydrogenase by nucleosides and nucleotides. *Biochem. Biophys. Res. Commun.* **435**, 202–208 (2013).
14. Luque, T. et al. Sorbitol dehydrogenase of *Drosophila*. Gene, protein, and expression data show a two-gene system. *J. Biol. Chem.* **273**, 34293–34301 (1998).
15. Bellen, H. J. et al. The *Drosophila* Gene Disruption Project: progress using transposons with distinctive site specificities. *Genetics* **188**, 731–743 (2011).
16. Bausenwein, B., Ditttrich, A. P. & Fischbach, K. F. The optic lobe of *Drosophila melanogaster*. II. Sorting of retinotopic pathways in the medulla. *Cell Tissue Res.* **267**, 17–28 (1992).
17. Kikkawa, R. et al. Effect of a new aldose reductase inhibitor, (E)-3-carboxymethyl-5-[(2E)-methyl-3-phenylpropenylidene]rhodanine (ONO-2235) on peripheral nerve disorders in streptozotocin-diabetic rats. *Diabetologia* **24**, 290–292 (1983).
18. Matsumoto, T. et al. Long-term treatment with ranirestat (AS-3201), a potent aldose reductase inhibitor, suppresses diabetic neuropathy and cataract formation in rats. *J. Pharmacol. Sci.* **107**, 340–348 (2008).
19. Ramirez, M. A. & Borja, N. L. Epalrestat: an aldose reductase inhibitor for the treatment of diabetic neuropathy. *Pharmacotherapy* **28**, 646–655 (2008).
20. Hao, W. et al. Hyperglycemia promotes Schwann cell de-differentiation and de-myelination via sorbitol accumulation and Igf1 protein down-regulation. *J. Biol. Chem.* **290**, 17106–17115 (2015).
21. Grewal, A. S., Bhardwaj, S., Pandita, D., Lather, V. & Sekhon, B. S. Updates on aldose reductase inhibitors for management of diabetic complications and non-diabetic diseases. *Mini Rev. Med. Chem.* **16**, 120–162 (2016).
22. Chalk, C., Benstead, T. J. & Moore, F. Aldose reductase inhibitors for the treatment of diabetic polyneuropathy. *Cochrane Database Syst. Rev.* **17**, CD004572 (2007).
23. Polydefkis, M. et al. Safety and efficacy of ranirestat in patients with mild-to-moderate diabetic sensorimotor polyneuropathy. *J. Peripher. Nerv. Syst.* **20**, 363–371 (2015).
24. Sekiguchi, K. et al. Aldose reductase inhibitor ranirestat significantly improves nerve conduction velocity in diabetic polyneuropathy: a randomized double-blind placebo-controlled study in Japan. *J. Diabetes Investig.* **10**, 466–474 (2019).
25. Züchner, S. et al. Mutations in the mitochondrial GTPase mitofusin 2 cause Charcot-Marie-Tooth neuropathy type 2A. *Nat. Genet.* **36**, 449–451 (2004).
26. De Vos, M., Hayward, B. E., Picton, S., Sheridan, E. & Bonthon, D. T. Novel PMS2 pseudogenes can conceal recessive mutations causing a distinctive childhood cancer syndrome. *Am. J. Hum. Genet.* **74**, 954–964 (2004).
27. Rumsby, G., Carroll, M. C., Porter, R. R., Grant, D. B. & Hjelm, M. Deletion of the steroid 21-hydroxylase and complement C4 genes in congenital adrenal hyperplasia. *J. Med. Genet.* **23**, 204–209 (1986).
28. Chen, J.-M., Cooper, D. N., Chuzhanova, N., Férec, C. & Patrinos, G. P. Gene conversion: mechanisms, evolution and human disease. *Nat. Rev. Genet.* **8**, 762–775 (2007).
29. Harel, T. et al. Recurrent de novo and biallelic variation of ATAD3A, encoding a mitochondrial membrane protein, results in distinct neurological syndromes. *Am. J. Hum. Genet.* **99**, 831–845 (2016).
30. Lupski, J. R. et al. DNA duplication associated with Charcot-Marie-Tooth disease type 1A. *Cell* **66**, 219–232 (1991).
31. Schmidt, R. E. et al. Inhibition of sorbitol dehydrogenase exacerbates autonomic neuropathy in rats with streptozotocin-induced diabetes. *J. Neuropathol. Exp. Neurol.* **60**, 1153–1169 (2001).
32. Schmidt, R. E. et al. A potent sorbitol dehydrogenase inhibitor exacerbates sympathetic autonomic neuropathy in rats with streptozotocin-induced diabetes. *Exp. Neurol.* **192**, 407–419 (2005).
33. Obrosova, I. G. Increased sorbitol pathway activity generates oxidative stress in tissue sites for diabetic complications. *Antioxid. Redox Signal.* **7**, 1543–1552 (2005).
34. Sango, K. et al. High glucose-induced activation of the polyol pathway and changes of gene expression profiles in immortalized adult mouse Schwann cells IMS32. *J. Neurochem.* **98**, 446–458 (2006).
35. Holmes, R. S., Duley, J. A. & Hilgers, J. Sorbitol dehydrogenase genetics in the mouse: a “null” mutant in a “European” C57BL strain. *Anim. Blood Groups Biochem. Genet.* **13**, 263–272 (1982).
36. Lee, A. Y., Chung, S. K. & Chung, S. S. Demonstration that polyol accumulation is responsible for diabetic cataract by the use of transgenic mice expressing the aldose reductase gene in the lens. *Proc. Natl Acad. Sci. USA* **92**, 2780–2784 (1995).
37. Ng, T. F. et al. Effects of sorbitol dehydrogenase deficiency on nerve conduction in experimental diabetic mice. *Diabetes* **47**, 961–966 (1998).
38. Ruff, J. S. et al. Human-relevant levels of added sugar consumption increase female mortality and lower male fitness in mice. *Nat. Commun.* **4**, 2245 (2013).
39. Callaghan, B. C., Cheng, H. T., Stables, C. L., Smith, A. L. & Feldman, E. L. Diabetic neuropathy: clinical manifestations and current treatments. *Lancet Neurol.* **11**, 521–534 (2012).
40. Dyck, P. J. et al. The prevalence by staged severity of various types of diabetic neuropathy, retinopathy, and nephropathy in a population-based cohort: the Rochester Diabetic Neuropathy Study. *Neurology* **43**, 817–824 (1993).
41. Lorenzi, M. The polyol pathway as a mechanism for diabetic retinopathy: attractive, elusive, and resilient. *Exp. Diabetes Res.* **2007**, 61038 (2007).

Publisher's note Springer Nature remains neutral with regard to jurisdictional claims in published maps and institutional affiliations.

© The Author(s), under exclusive licence to Springer Nature America, Inc. 2020

Inherited Neuropathy Consortium

Aixa Rodriguez²⁵, Alexa Bacha⁷, Ashley Kosikowski²⁶, Beth Wood¹¹, Brett McCray²⁷, Brianna Blume²⁸, Carly Siskind²⁹, Charlotte Sumner²⁷, Daniela Calabrese¹⁰, David Walk³⁰, Dragan Vujovic¹⁵, Eun Park²⁷, Francesco Muntoni², Gabrielle Donlevy³¹, Gyula Acsadi²⁶, John Day²⁹, Joshua Burns³¹, Jun Li³², Karen Krajewski³, Kate Eichinger¹¹, Kayla Cornett³¹, Krista Mullen³⁰, Perez Quiros Laura⁷, Laurie Gutmann⁷, Maria Barrett²⁸, Mario Saporta³³, Mariola Skorupinska², Natalie Grant³⁴, Paula Bray³¹, Reza Seyedsadjadi³⁴, Riccardo Zuccarino⁷, Richard Finkel²⁵, Richard Lewis³⁵, Rosemary R. Shy³⁶, Sabrina Yum³⁷, Sarah Hilbert³⁰, Simone Thomas²⁷, Steffen Behrens-Spraggins¹¹, Tara Jones³⁵, Thomas Lloyd²⁷, Tiffany Grider⁷, Tim Estilow³⁶ and Vera Fridman²⁸

²⁵Department of Pediatrics, Division of Neurology, Nemours Children's Hospital, Orlando, FL, USA. ²⁶Neurology, Charcot-Marie-Tooth Center of Excellence, Connecticut Children's Medical Center, Hartford, CT, USA. ²⁷Department of Neurology, Johns Hopkins University, Baltimore, MD, USA. ²⁸University of Colorado Health Neurosciences Center, Aurora, CO, USA. ²⁹Department of Neurology and Neurological Sciences, Stanford University, Stanford, CA, USA. ³⁰Department of Neurology, University of Minnesota, Minneapolis, MN, USA. ³¹Paediatric Gait Analysis Service of NSW, The Children's Hospital at Westmead, Westmead, New South Wales, Australia. ³²Department of Neurology, Neuromuscular and Inherited Neuropathies Division, Wayne State University School of Medicine, Detroit, MI, USA. ³³Department of Neurology, Neuromuscular Division, University of Miami Miller School of Medicine, Miami, FL, USA. ³⁴Department of Neurology, Harvard/Massachusetts General Hospital, Boston, MA, USA. ³⁵Department of Neurology, Cedars-Sinai Medical Center, Los Angeles, CA, USA. ³⁶Department of Pediatrics, Carver College of Medicine, University of Iowa, Iowa City, IA, USA. ³⁷Department of Neurology, Children's Hospital of Philadelphia, Philadelphia, PA, USA.

Methods

Patients. For the initial discovery study, we enrolled 598 individuals who previously underwent WES or WGS with a clinical diagnosis of CMT, collected through the collaborative initiative Inherited Neuropathy Consortium, which recruits patients from 15 sites in the United States and the United Kingdom. An additional 400 individuals with a clinical diagnosis of sporadic or recessive dHMN or CMT2 and negative for the known genetic defects associated with the disease were collected across additional centres in the United Kingdom, Italy, Kuwait, Saudi Arabia and China. The study has received ethical approval (INC 6602), and all individuals gave written informed consent to participate. The study has complied with all relevant ethical regulations.

Disease severity was scored using the previously validated CMTNSv2 score or the CMT examination score (CMTEsv2)¹¹ and cases were divided into mild (CMTNS 0 to 10 or CMTEs 0 to 7), moderate (CMTNS 11 to 20 or CMTEs 8 to 16) and severe (CMTNS 21 to 36 or CMTEs 17 to 28). In individuals for which CMTNS or CMTEs scores had not been collected, the disease was considered mild if walking was possible without aid, moderate if walking was possible with foot orthosis or ankle dorsiflexion was less than MRC grade 3, and severe if patients needed a walking aid, such as a stick, or a wheelchair.

WES and WGS. WES was performed in 598 index individuals from families with sporadic and recessive CMT and dHMN. The SureSelect Human All Exon 50 MB Kit (Agilent) was used for in-solution enrichment, and the HiSeq 2500 instrument (Illumina) was used to produce ~120-base-pair paired-end sequence reads. The Burrows–Wheeler aligner and FreeBayes were used to align sequence reads and call variants. Final data were uploaded into GENESIS software for analysis (<https://www.genesis-app.com>). A filtering approach to search for families sharing the same homozygous variants was applied across all exomes in the database. Variants were prioritized on the basis of segregation, MAF <0.0001 in the 1000 Genomes Project⁷, NHLBI GO Exome Sequencing project (Exome Variant Server, NHLBI GO Exome Sequencing Project, Seattle, WA (<http://evs.gs.washington.edu/EVS/>) (September 2017) or gnomAD⁸.

PCR and Sanger sequencing of *SORD* and *SORD2P*. Coding exons and flanking introns of *SORD* and exon 7 of *SORD2P* were amplified from genomic DNA by PCR followed by Sanger sequencing. If necessary, an internal distinct primer was used for sequencing. The primer sequences, concentrations and PCR thermocycling conditions are provided in Supplementary Table 1. Sanger sequencing was performed by Eurofins Genomics USA or Source Bioscience.

Fibroblast cultures. A skin biopsy was performed for fibroblast culture in four patients carrying biallelic c.757delG (p.Ala253GlnfsTer27) variants (individual II of family 4, family 7, family 9 and family 16) and one patient carrying one heterozygous c.757delG (p.Ala253GlnfsTer27) variant and one additional nonsense c.895C>T (p.Arg299Ter) variant, two unaffected individuals carrying the c.757delG (p.Ala253GlnfsTer27) variant (individuals I-1 and I-2 of family 4) and five age- and sex-matched controls.

Fibroblasts were cultured in Dulbecco's modified Eagle's medium (ThermoFisher) supplemented with 10% fetal bovine serum, penicillin and streptomycin (Gibco). Cells were grown in 5% CO₂ at 37°C in a humidified incubator. Asynchronous cell cultures were grown to approximately 80% confluency, and then treated with epalrestat (100 μM), ranirestat (10 μM) or DMSO for 72 h. The medium containing the drugs or DMSO was changed every 24 h.

Western blotting. Fibroblasts were lysed in RIPA buffer (ThermoFisher) containing protease inhibitors (Roche) and sonicated for 5 min with the Bioruptor sonication device (Diagenode). Cell lysates were centrifuged at 13,000g for 10 min at 4°C, and the supernatant was collected for protein quantification (Pierce BCA Protein Assay Kit). A 30-μg quantity of protein sample was mixed with Bolt LDS Sample Buffer and Sample Reducing Agent (ThermoFisher) and heated at 90°C for 5 min. Samples were loaded on a Bolt 4–12% Bis-Tris Plus mini-gel followed by transfer onto a nitrocellulose membrane (Bio-Rad). The membrane was blocked with 5% non-fat milk and incubated with anti-SORD (1:1,000 dilution, ab189248, Abcam) antibody for 2 h, washed with Tris-buffered saline containing 0.01% Tween 20 (Bio-Rad) and incubated with a peroxidase-conjugated anti-rabbit antibody (1:2,500 dilution, catalog no. 7074, Cell Signaling). The membrane was subsequently incubated with monoclonal antibody against tubulin (1:1,000 dilution, Santa Cruz) and secondary anti-mouse antibody (1:2,500 dilution, catalog no. 7076, Cell Signaling). Chemoluminescence detection was performed with the SuperSignal West Pico PLUS Chemiluminescent Substrate and imaged with the FluorChem E (ProteinSimple).

Sorbitol measurement in human fibroblast lysates and serum. Sorbitol determination from lysates of human fibroblasts was performed by UPLC–tandem mass spectrometry (MS/MS) (Waters Acquity UPLC & TQD mass spectrometer). Fibroblasts were collected and lysed as described in the section on western blotting, but in the absence of proteinase inhibitor, which contains mannitol, a sorbitol enantiomer that can interfere with UPLC–MS/MS sorbitol determination. The lysate samples underwent protein precipitation with acetonitrile (1:5), tenfold

dilution with acetonitrile/water (50:50) and cleanup on Oasis HLB cartridges (10 mg/1 ml), before injection (3 μl) into the UPLC system. The UPLC conditions were as follows: column, BEH amide 1.7 μm (2.1 × 100 mm) at 88°C; eluent A, acetonitrile 90%/water 5%/isopropanol 5%; eluent B, acetonitrile 80%/water 20%; gradient elution, 0 min 100% A to 3.6 min 100% B; flow rate, 0.45 ml min⁻¹. The retention time of sorbitol was 2.7 min. The linearity of the method was assessed between 0.25 and 50 mg l⁻¹. The MS/MS conditions were as follows: interface, electrospray interface in negative ion mode; multiple reaction monitoring acquisition, *m/z* 180.9 → 88.9 (CV 24, CE 15). The detection limit (signal-to-noise ratio = 3) was 0.03 mg l⁻¹.

For fasting sorbitol level testing, blood was collected after overnight fasting (last meal the evening before) in serum separator tubes. Samples were centrifuged at 500g for 10 min, and serum was separated and frozen within 1 h from blood collection. The sorbitol level was tested by UPLC using a method adapted from Li et al.⁴². The conditions were as follows: column, BEH amide 1.7 μm maintained at 25°C (instead of 45°C); eluent A, 10 mM ammonium acetate pH 10; eluent B, acetonitrile; flow rate, 0.6 ml min⁻¹ with the same gradient. The retention time of sorbitol was 6.0 min. The MS/MS conditions were the same as for the fibroblast analysis. The serum samples underwent protein precipitation with cold methanol (1:5), fivefold dilution with acetonitrile/water (50:50) and cleanup on Oasis HLB cartridges (10 mg/1 ml), before injection (3 μl) into the UPLC system. The calibration curve was prepared in serum in the sorbitol concentration range 0.1–20 mg l⁻¹.

***Drosophila* stocks and experimental procedures.** Unless specified otherwise, all of the flies were kept on cornmeal–molasses–yeast medium at 25°C, 65% humidity, with 12 h light/12 h dark cycles. The following fly strains used in this study were obtained from the Bloomington *Drosophila* Stock Center: *elav^{C155}-GAL4*, *GMR-GAL4*, *Sodh2^{MBO1265}*, *UAS-Sodh1 RNAi* and *UAS-Sodh2 RNAi*. Epalrestat or ranirestat was dissolved in DMSO to achieve a stock concentration of 10 mg ml⁻¹, and then mixed into 10 ml fly food at a final concentration of 80 μg ml⁻¹. An equal amount of DMSO was mixed into the fly food as a control. The vials were dried at room temperature for 12 h before feeding.

***Drosophila* lifespan assay and negative geotaxis assay.** For the lifespan assay, 100 newly eclosed female flies from each group were collected and placed in vials of 20 individuals. The flies were transferred into new vials every 2 d and the number of dead flies was counted. Survival data were plotted using a Kaplan–Meier plot and compared between groups using a log-rank test. For the negative geotaxis behavior assay, 10 age-matched female flies were placed in a vial marked with a black line drawn horizontally 8 cm above the bottom. The flies were given 60 min to fully recover from CO₂ anesthesia, and then gently tapped onto the bottom and given 10 s to climb. Flies that crossed the 8-cm line were counted. For each vial, this assay was repeated 10 times, and 8–10 independent vials of each group (a total of 80–100 flies per group) were tested. To minimize observer-expectancy bias, this assay was performed with the examiner masked to the group assignment.

***Drosophila* brain immunostaining, imaging and quantification.** Fly brains were dissected in phosphate-buffered saline (PBS, pH 7.4), fixed in 4% formaldehyde for 10 min and washed in PBS containing 0.4% v/v Triton X-100 (PBXT) 3 times (15 min each). The brains were then incubated with primary mouse anti-BRP antibody (nc82, Developmental Studies Hybridoma Bank) at 1:250 dilution in 0.4% PBXT with 5% normal goat serum at 4°C overnight with gentle shaking. The brains were incubated with Alexa Fluor 555-conjugated anti-mouse secondary antibody (ThermoFisher) and Cy5-conjugated anti-HRP (Jackson ImmunoLab) at 1:250 dilution at 4°C overnight with gentle shaking, followed by DAPI (1:300, Invitrogen) staining at room temperature for 10 min. The samples were mounted on glass slides with VECTASHIELD Antifade Mounting Medium (Vector Laboratories). Brain slides were imaged using an Olympus IX81 confocal microscope with an ×60 oil immersion objective lens with a scan speed of 8.0 μs per pixel and spatial resolution of 1,024 × 1,024 pixels. Images were processed using FluoView 10-ASW (Olympus). Quantification of the number and size of the vacuole-like structures was carried out using ImageJ/Fiji (version 1.52n). A total of 3–8 laminae (*x-y* plane as shown in Fig. 3b) of each group were used.

Statistical analyses. Clinical variables were reported as mean ± s.d. (min–max) (continuous variables) and percentages (categorical variables). Continuous variables from experimental measurements were compared with a two-tailed Student's *t*-test or a two-way ANOVA followed by a post hoc Tukey's multiple-comparison test, as specified in the main text and figures. *P* values < 0.05 were considered to be significant.

Reporting Summary. Further information on research design is available in the Nature Research Reporting Summary linked to this article.

Data availability

All data described in this paper are present either in the main text or in the Supplementary Information. Source data for Fig. 2 are presented with the paper. The sequence data obtained by WES and WGS are not publicly available because the study participants did not give full consent for releasing data publicly.

References

42. Li, L. et al. The induction of trehalose and glycerol in *Saccharomyces cerevisiae* in response to various stresses. *Biochem. Biophys. Res. Commun.* **387**, 778–783 (2009).

Acknowledgements

This project was supported by the NINDS (R01NS075764 to S.Z. and M.S.; R01NS105755 to S.Z.), the NIH (R21GM119018 and 1R61AT010408 to R.G.Z.), the NCATS (U54NS065712 to M.S.), the CMT Association, the Hereditary Neuropathy Foundation, The Genesis Project foundation, the Muscular Dystrophy Association, the European Union's Horizon 2020 research and innovation programme under the ERA-NET Cofund action no. 643578 under the frame of the E-Rare-3 network PREPARE (01GM1607 to M.S.; and unfunded to S.Z.), the grant 779257 'Solve-RD' (to R.S. and M.S., M.M.R. and H.H.) and the National Institute for Health Research University College London Hospitals Biomedical Research Centre (to M.L.). The project received further support from the 'Bundesministerium für Bildung und Forschung' (BMBF) via funding for the TreatHSP consortium (01GM1905 to R.S.) and the National Institutes of Health (grant 5R01NS072248 to R.S. and S.Z.), the Austrian Science Fund (FWF, P27634FW to M.A.-G.) and the National Natural Science Foundation of China (81771366). A.C. thanks the Medical Research Council (MR/T001712/1), the Wellcome Trust (204841/Z/16/Z), the Fondazione CARIPIO (2019-1836), the Italian Ministry of Health Ricerca Corrente 2018–2019 and the Inherited Neuropathy Consortium (INC) for grant support. H.H. and M.M.R. thank the MRC, the Wellcome Trust, the MDA, MD UK, Ataxia UK, The MSA Trust, the Rosetrees Trust and the NIHR UCLH BRC for grant support. A.M.R. is funded by a Wellcome Trust Postdoctoral Fellowship for Clinicians (110043/Z/15/Z). D.N.H. receives grant support through NIH U54

NS065712-09, the Muscular Dystrophy Association, the Friedreich's Ataxia Alliance and Voyager Pharmaceuticals. We thank M. Tekin for kindly providing DNA from healthy controls or Turkish ancestry. We also thank Twenty Three Calvin (Marie Stargala and Matthew Rosen) for creating the cover art for the issue.

Author contributions

Conceptualization: A.C. and S.Z. Funding acquisition: S.Z., M.E.S., M.M.R., H.H., R.S. and M.S., Investigation: A.C., Y.Z., A.P.R., S.N., S.C., M.P., E.Buglo, R.G.Z. and S.Z. Resources: A.C., Y.Z., A.P.R., S.N., S.C., L.A., A.A.-A, M.A.-G., C.J.B., Y.B., D.M.B.-B., E.Bugiardini, J.D., M.C.D., S.M.E.F., A.A.-F., E.G., M.A.A., S.A.H., N.A.H., H.H., R.I., A.K., M.L., Z.L., S.M., T.M., F.M., E.M., D.P., M.P., C.P., E.P., A.M.R., L.S., S.S.S., R.S., J.E.S., T.S., M.S., P.S., B.T., F.T., S.T., J.V., R.Z., D.N.H., M.M.R., M.E.S., R.G.Z. and S.Z. Supervision: S.Z. and R.G.Z. Writing—original draft: A.C., Y.Z., A.P.R., R.G.Z. and S.Z. All authors contributed to revising the manuscript.

Competing interests

The authors declare no competing interests.

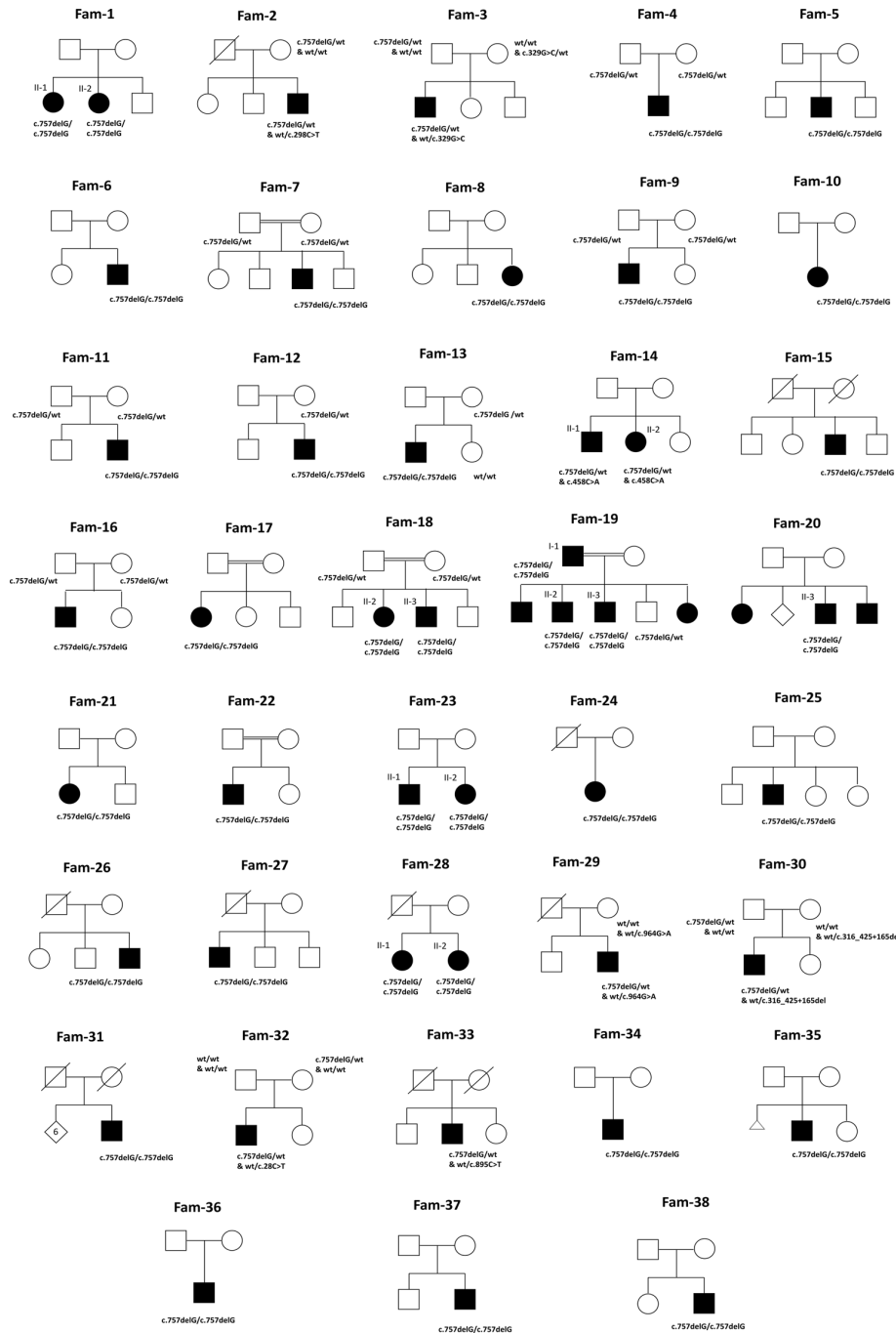
Additional information

Extended data is available for this paper at <https://doi.org/10.1038/s41588-020-0615-4>.

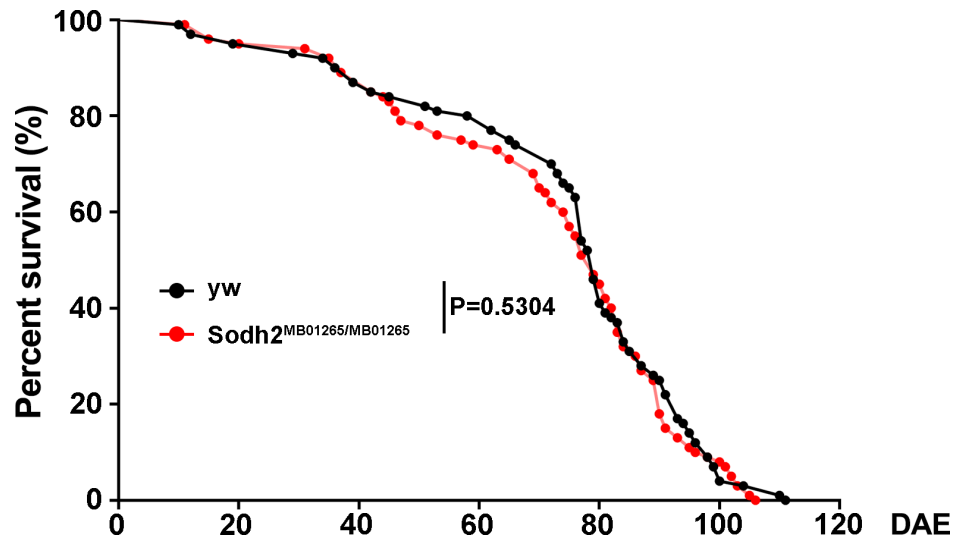
Supplementary information is available for this paper at <https://doi.org/10.1038/s41588-020-0615-4>.

Correspondence and requests for materials should be addressed to A.C., R.G.Z. or S.Z.

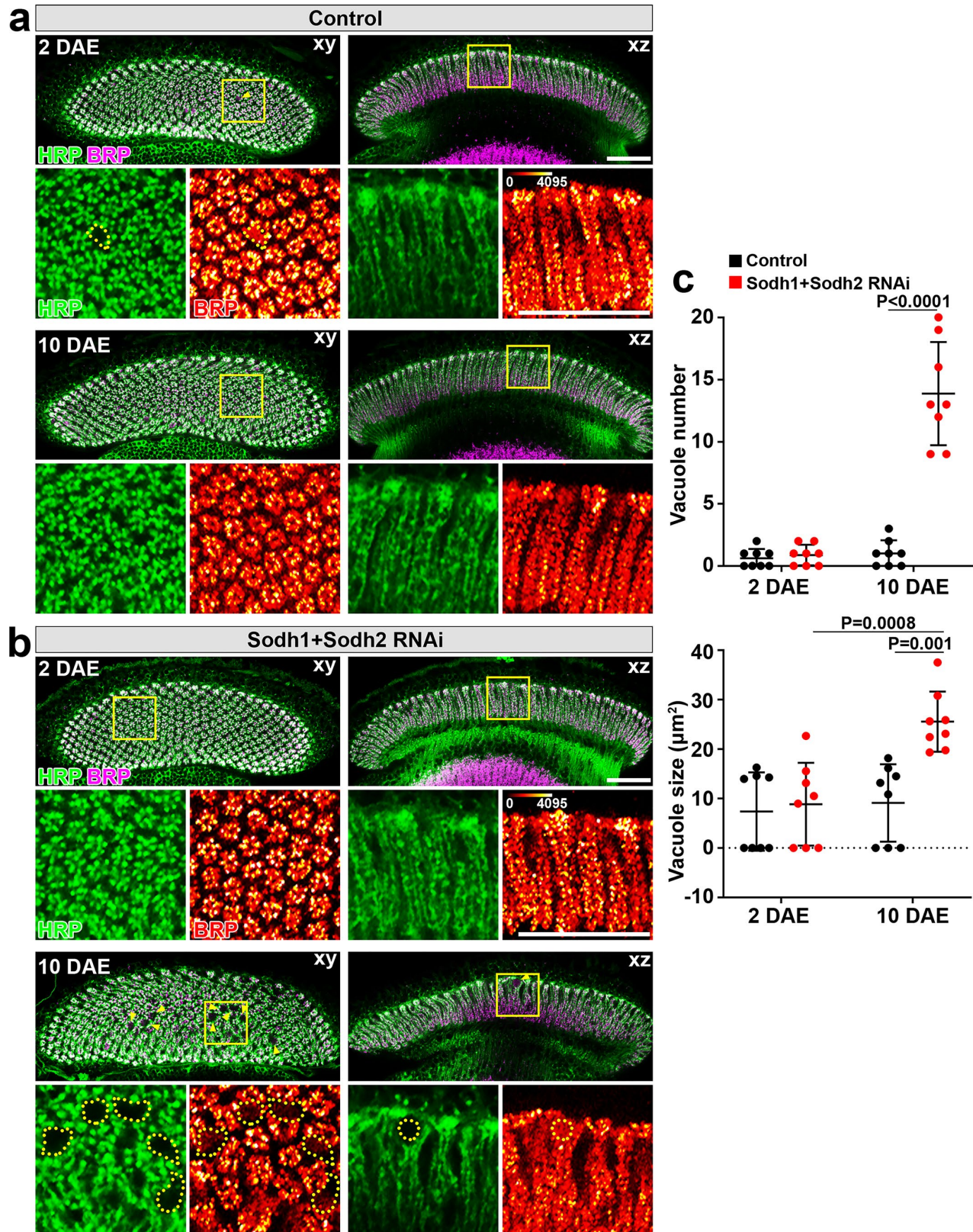
Reprints and permissions information is available at www.nature.com/reprints.



Extended Data Fig. 1 | Pedigrees of families carrying biallelic mutations in *SORD*. The squares indicate males, the circles females, and the diagonal lines deceased individuals. Patients are indicated with filled shapes. Genotypes are provided when tested by Sanger sequencing.

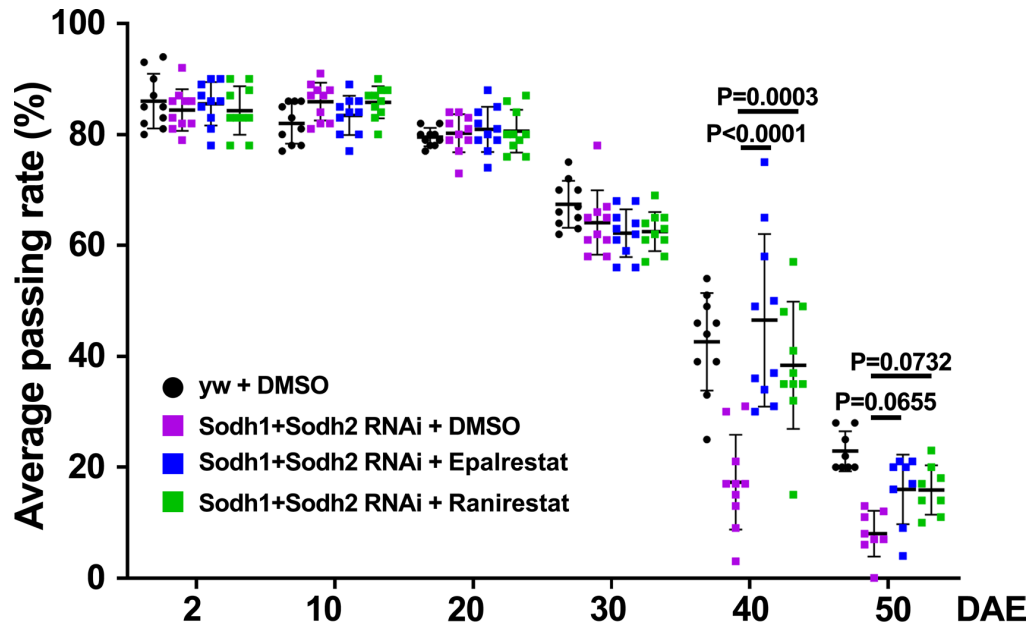


Extended Data Fig. 2 | Loss of *Drosophila* Sodh does not affect life span. Life span of control flies (*yw*) and *Sodh2*^{MB01265/MB01265} flies. Data are shown in Kaplan-Meier survival plot. $n=100$ biologically independent animals. Significance level was established by a two-sided log-rank test.



Extended Data Fig. 3 | See next page for caption.

Extended Data Fig. 3 | Double knockdown of *Drosophila Sodh1* and *Sodh2* causes age-dependent synaptic degeneration. **a,b**, Laminae of control (*GMR-GAL4* heterozygotes) or *Sodh1* and *Sodh2* double knockdown homozygous flies at 2 DAE and 10 DAE were stained with HRP (green; marks neuronal membranes) and BRP (magenta; marks synaptic active zones). Yellow arrowheads indicate vacuole-like structures in the lamina that correspond to missing terminals. The areas outlined by yellow boxes are shown at higher magnification. The intensity of BRP is indicated using a red spectrum. Dotted lines indicate the area of lamina vacuole-like structures. Scale bars: 30 μm . **c**, Quantification of the number and size of vacuole-like structures. $n = 8$ biologically independent samples. Data are presented as mean \pm s.d. (error bars). Statistical analysis was performed using two-way ANOVA followed by post-hoc Tukey's multiple comparison test.



Extended Data Fig. 4 | Treatment with aldose reductase inhibitors Epalrestat and Ranirestat restore locomotor function in Sodh1 and Sodh2 double knockdown flies. Locomotor activity of control flies (*yw*) feeding with DMSO, or flies with neuronal-specific knockdown of *Sodh1* and *Sodh2* feeding with DMSO, 80 $\mu\text{g}/\text{ml}$ Epalrestat, or 80 $\mu\text{g}/\text{ml}$ Ranirestat. $n=10$ in 2, 10, 20, 30, 40 DAE, and $n=8$ in 50 DAE. Data are presented as mean \pm s.d. (error bars). Statistical analysis was performed using two-way ANOVA followed by post-hoc Tukey's multiple comparison test.

Reporting Summary

Nature Research wishes to improve the reproducibility of the work that we publish. This form provides structure for consistency and transparency in reporting. For further information on Nature Research policies, see [Authors & Referees](#) and the [Editorial Policy Checklist](#).

Statistics

For all statistical analyses, confirm that the following items are present in the figure legend, table legend, main text, or Methods section.

- | | |
|-------------------------------------|--|
| n/a | Confirmed |
| <input type="checkbox"/> | <input checked="" type="checkbox"/> The exact sample size (n) for each experimental group/condition, given as a discrete number and unit of measurement |
| <input type="checkbox"/> | <input checked="" type="checkbox"/> A statement on whether measurements were taken from distinct samples or whether the same sample was measured repeatedly |
| <input type="checkbox"/> | <input checked="" type="checkbox"/> The statistical test(s) used AND whether they are one- or two-sided
<i>Only common tests should be described solely by name; describe more complex techniques in the Methods section.</i> |
| <input type="checkbox"/> | <input checked="" type="checkbox"/> A description of all covariates tested |
| <input type="checkbox"/> | <input checked="" type="checkbox"/> A description of any assumptions or corrections, such as tests of normality and adjustment for multiple comparisons |
| <input type="checkbox"/> | <input checked="" type="checkbox"/> A full description of the statistical parameters including central tendency (e.g. means) or other basic estimates (e.g. regression coefficient) AND variation (e.g. standard deviation) or associated estimates of uncertainty (e.g. confidence intervals) |
| <input type="checkbox"/> | <input checked="" type="checkbox"/> For null hypothesis testing, the test statistic (e.g. F , t , r) with confidence intervals, effect sizes, degrees of freedom and P value noted
<i>Give P values as exact values whenever suitable.</i> |
| <input checked="" type="checkbox"/> | <input type="checkbox"/> For Bayesian analysis, information on the choice of priors and Markov chain Monte Carlo settings |
| <input checked="" type="checkbox"/> | <input type="checkbox"/> For hierarchical and complex designs, identification of the appropriate level for tests and full reporting of outcomes |
| <input checked="" type="checkbox"/> | <input type="checkbox"/> Estimates of effect sizes (e.g. Cohen's d , Pearson's r), indicating how they were calculated |

Our web collection on [statistics for biologists](#) contains articles on many of the points above.

Software and code

Policy information about [availability of computer code](#)

Data collection HiSeq 2500 (Illumina), ABI 3730xl genetic analyser (Applied Biosystems, Foster City, CA, USA), FluorChem E (ProteinSimple), Acquity UPLC & TQD mass spectrometer (Waters, Milford, MA, USA), Olympus IX81 confocal microscope (Olympus)

Data analysis Burrows-Wheeler Aligner, Freebayes, GENESIS software for analysis (genesis-app.com), FluoView10-ASW v 04.02.02.09 (Olympus, Tokyo, Japan), GraphPad Prism v7 Software (San Diego, CA, USA), Fiji 1.52p (NIH, USA), STATA (v 13.1), TargetLynx/MassLynx v4.1 (Waters, Milford, MA, USA), Image Lab 6.0.1 (BioRad, Hercules, CA, USA)

For manuscripts utilizing custom algorithms or software that are central to the research but not yet described in published literature, software must be made available to editors/reviewers. We strongly encourage code deposition in a community repository (e.g. GitHub). See the Nature Research [guidelines for submitting code & software](#) for further information.

Data

Policy information about [availability of data](#)

All manuscripts must include a [data availability statement](#). This statement should provide the following information, where applicable:

- Accession codes, unique identifiers, or web links for publicly available datasets
- A list of figures that have associated raw data
- A description of any restrictions on data availability

The sequence data obtained by whole-exome and whole-genome sequencing are not publicly available because study participants did not give full consent for releasing data publicly. Since whole-exome and whole-genome sequence data are protected by the Personal Information Protection Law, availability of these data is under the regulation by the institutional review board.

Field-specific reporting

Please select the one below that is the best fit for your research. If you are not sure, read the appropriate sections before making your selection.

Life sciences Behavioural & social sciences Ecological, evolutionary & environmental sciences

For a reference copy of the document with all sections, see [nature.com/documents/nr-reporting-summary-flat.pdf](https://www.nature.com/documents/nr-reporting-summary-flat.pdf)

Life sciences study design

All studies must disclose on these points even when the disclosure is negative.

Sample size	<p>PATIENTS All available DNA samples from patients with inherited neuropathy/CMT were considered for mutations in SORD gene. These numbers were considered sufficient as they had enabled the previous discovery of multiple genes associated with CMT</p> <ul style="list-style-type: none"> - 598 undiagnosed CMT patients who underwent WES or WGS at the University of Miami, FL, USA and available on Genesis platform - 103 unresolved CMT cases who underwent WES or WGS at the UCL Queen Square Institute of Neurology, London, UK - 297 recessive or sporadic CMT patients (without previous WGS or WGS) were tested by Sanger sequencing targeting exon 7 of SORD gene <p>Also we included as controls</p> <p>CONTROLS</p> <ul style="list-style-type: none"> - 600 internal healthy controls, including 300 samples of European, 100 samples of Turkish and 200 samples of Middle Eastern origin who were tested by anger sequencing targeting exon 7 of SORD gene - 4590 subjects affected by other neurological conditions who underwent WES or WGS at the University of Miami, FL, USA and available on Genesis platform - 142,588 genomes from healthy controls on gnomAD v3 database <p>Although not reported in the manuscript, we specify here that frequency of biallelic mutations in SORD in CMT patients (45 out of 998 undiagnosed CMT cases) significantly higher than in controls (0 out of 600 internal healthy controls DNAs; 0 out of 4590 WES/WGS from subjects affected by other neurological conditions, 1 out of 142,588 genomes from healthy controls on gnomAD v3 database) - $p < 0.001$ for all comparisons by Fisher's test</p> <p>Additionally, we tested the fasting serum sorbitol level from 10 patients with biallelic c.753delG; p.Ala253GlnfsTer27 mutation in SORD and 10 healthy controls was tested</p>
Data exclusions	no data were excluded from the analysis
Replication	All experiments involving Sanger sequencing, western blotting, sorbitol measurement and Drosophila model characterization were repeated independently twice and all attempts at replication were successful.
Randomization	Randomization is not relevant to this study. Both patients with CMT or and controls were tested for the presence of mutations in SORD gene
Blinding	For characterization of Drosophila model, examiners (either G.R.Z. or Y.Z) were blinded to the affection and/or treatment status of the flies. For sorbitol quantification, examiners (S.N. and E.G.) were blinded to the affection status of the samples.

Reporting for specific materials, systems and methods

We require information from authors about some types of materials, experimental systems and methods used in many studies. Here, indicate whether each material, system or method listed is relevant to your study. If you are not sure if a list item applies to your research, read the appropriate section before selecting a response.

Materials & experimental systems

- | n/a | Involved in the study |
|-------------------------------------|---|
| <input type="checkbox"/> | <input checked="" type="checkbox"/> Antibodies |
| <input checked="" type="checkbox"/> | <input type="checkbox"/> Eukaryotic cell lines |
| <input checked="" type="checkbox"/> | <input type="checkbox"/> Palaeontology |
| <input type="checkbox"/> | <input checked="" type="checkbox"/> Animals and other organisms |
| <input type="checkbox"/> | <input checked="" type="checkbox"/> Human research participants |
| <input checked="" type="checkbox"/> | <input type="checkbox"/> Clinical data |

Methods

- | n/a | Involved in the study |
|-------------------------------------|---|
| <input checked="" type="checkbox"/> | <input type="checkbox"/> ChIP-seq |
| <input checked="" type="checkbox"/> | <input type="checkbox"/> Flow cytometry |
| <input checked="" type="checkbox"/> | <input type="checkbox"/> MRI-based neuroimaging |

Antibodies

Antibodies used

1. anti-SORD (1:1000 dilution, ab189248, Abcam).
2. anti-tubulin (1:1000 dilution, D-10 sc-5274, Santa Cruz).
3. peroxidase-conjugated anti-rabbit antibody (1:2500 dilution, Cat. #7074, Cell Signaling)

4. peroxidase-conjugated anti-mouse antibody (1:2500 dilution, Cat. #7076, Cell Signaling).
5. anti-BRP antibody (1:250 dilution, Developmental Studies Hybridoma Bank, Cat. #nc82).
6. Alexa Fluor 555-conjugated anti-mouse secondary antibody (1:250 dilution, Thermo Fisher Scientific, Cat. #A21422).
7. Cy5-conjugated anti-HRP (1:250 dilution, Jackson ImmunoLab, Cat. #123-175-021).

Validation

- As is stated on the manufacturers' website, each primary antibody has been individually validated to react against human protein
1. anti-SORD validated for immunoprecipitation and Western blotting
 2. anti-tubulin validated Western Blotting, immunoprecipitation, immunofluorescence, immunohistochemistry and solid phase ELISA
 3. peroxidase-conjugated anti-rabbit antibody validated for Western Blotting
 4. peroxidase-conjugated anti-mouse antibody validated for Western Blotting
 5. anti-BRP antibody (nc82) validated for immunofluorescent staining
 6. Alexa Fluor 555-conjugated anti-mouse secondary antibody for immunofluorescent staining
 7. Cy5-conjugated anti-HRP for immunofluorescent staining

Animals and other organisms

Policy information about [studies involving animals](#); [ARRIVE guidelines](#) recommended for reporting animal research

Laboratory animals	Drosophila melanogaster
Wild animals	N/A
Field-collected samples	N/A
Ethics oversight	N/A

Note that full information on the approval of the study protocol must also be provided in the manuscript.

Human research participants

Policy information about [studies involving human research participants](#)

Population characteristics	<p>Patients are diagnosed with inherited neuropathy (CMT, dHMN). Controls were 600 subject (300 Europeans, 100 Turkish and 200 Middle Easterners) and 4598 subjected affected by other neurological conditions who underwent WES or WGS at the University of Miami, FL, USA and available on Genesis platform of European ancestry. Gender ratio was ~1:1 both for patients and controls.</p> <p>For fasting serum sorbitol testing we included 10 cases with biallelic c.753delG; p.Ala253GlnfsTer27 mutation in SORD and 10 healthy controls</p>
Recruitment	<p>Patients were recruited at one of the sites of the Inherited Neuropathy Consortium (https://www.rarediseasesnetwork.org/cms/inc) and additional centres in Europe, Saudi Arabia, Kuwait and China. The world-wide recruitment of patients has minimized any selection bias.</p> <p>600 controls were available from the University of Miami and the UCL Queen Square Institute of Neurology</p>
Ethics oversight	<p>The study has received ethical approval (INC 6602) from the University of Miami and all subjects gave written informed consent to participate. The study has complied with all relevant ethical regulations.</p>

Note that full information on the approval of the study protocol must also be provided in the manuscript.